Structural transitions and relaxation processes during the epitaxial growth of ultrathin CaF_2 films on Si(111)

Carsten Deiter*
Hamburger Synchrotronstrahlungslabor (HASYLAB), Deutsches Elektronensynchrotron (DESY), Notkestr. 85, D-22603 Hamburg, Germany

Markus Bierkandt
Institut für Festkörperphysik, Universität Hannover, Appelstr. 2, D-30176 Hannover, Germany

Andreas Klust
Department of Chemistry, Massachusetts Institute of Technology, Cambridge, Massachusetts 02139, USA

Christian Kumpf
Institute of Bio- and Nanosystems 3, Research Center Jülich, D-52425 Jülich, Germany and Fundamentals of Future Information Technology, JARA, Germany

Yixi Su
Institute for Solid State Research, Research Center Jülich, D-52425 Jülich, Germany and Fundamentals of Future Information Technology, JARA, Germany

Oliver Bunk
Swiss Light Source, Paul Scherrer Institut, CH-5232 Villigen PSI, Switzerland

Robert Feidenhans'l
Nano-Science Center, Niels Bohr Institute, University of Copenhagen, Universitetsparken 5, DK-2100 Copenhagen, Denmark

Joachim Wollschläger†
Fachbereich Physik, Universität Osnabrück, Barbarastr. 7, D-49069 Osnabrück, Germany
(Received 3 March 2010; revised manuscript received 7 July 2010; published 31 August 2010)

The structure and morphology of ultrathin lattice matched CaF_2 films of very few monolayers thickness, which were deposited on Si(111) substrates by molecular-beam epitaxy, have been studied *in situ* by synchrotron based grazing incidence x-ray diffraction. Even for the thinnest investigated film of three monolayers thickness, the in-plane structure of the CaF_2 film is determined by a lateral separation in two domains: a pseudomorphic phase assuming the lateral lattice constant of the Si(111) substrate and a completely relaxed phase. Analysis of the crystal truncation rods verifies that both phases adopt the entire homogeneous CaF_2 film thickness. Therefore, we propose that atomic steps of the substrate bypass the nucleation barrier for the formation of (Shockley partial) dislocations so that the film starts to relax below the classical critical film thickness. While the relaxed phase assumes also the CaF_2 bulk lattice constant for the vertical direction, the vertical lattice constant of the pseudomorphic phase increases due to the compressive lateral strain at the interface. This vertical expansion of the pseudomorphic phase, however, is larger than expected from the elastic constants of the CaF_2 bulk. The fraction of the pseudomorphic CaF_2 phase decreases with increasing film thickness. The interface between the pseudomorphic CaF_2 phase and the Si(111) substrate is characterized by Ca on T_4 sites, a smaller distance between the Si(111) substrate and the CaF interface layer and an expanded layer distance between CaF interface layer and the completely stoichiometric CaF_2 film.

DOI: 10.1103/PhysRevB.82.085449 PACS number(s): 61.05.cp, 68.35.Ct, 68.55.aj, 68.55.J−

I. INTRODUCTION

Pushing the structural dimensions of electronic devices from the micrometer scale of microelectronic devices into the nanometer scale of nanoelectronic devices the semiconductor technology has a need for manufacturing smooth ultrathin films and multilayers with a homogeneous thickness of only a few atomic layers. Therefore lattice matched material systems are the key to face this challenge since it is expected that these films grow only with little strain so that it is expected that these structures are of high quality. For instance, resonant tunneling devices have extremely high demands on the quality of insulating films which serve as tunneling barriers so that the thickness of the insulating films has to be in the range of only a very few nanometers.

Here, the combination of insulating CaF_2 films (band gap $E_{gap}^{CaF_2}=12.1$ eV) with Si substrates (band gap $E_{gap}^{Si}=1.1$ eV) is promising due to the advantages of very similar lattice structure with cubic symmetry (fluorite and diamond, respectively) and lattice mismatch of only 0.58% at room temperature.[1,2] On one hand, CaF_2 films of homogeneous

thickness are formed on Si(111) substrates (laminar layer-by-layer growth mode)[3,4] due to the their lower surface free energy [2.81×10^{14} eV/cm^2 for CaF_2(111) and 7.74×10^{14} eV/cm^2 for Si(111) (Ref. 1)]. On the other hand, dewetting behavior has been observed for CaF_2/Si(001) due to the instability of the polar CaF_2(001) surface.[1] Thus resonant tunneling devices involving CaF_2 tunneling barriers are based on Si(111) substrates.

One example for a nanoelectronic device is the resonant tunneling diode (RTD) which shows negative differential resistance so that this device is of large interest in the field of terahertz electronics.[4] The functionality of CaF_2-Si(111)-based RTDs has been reported first for triple barrier CaF_2 structures which terminate metallic $CoSi_2$ quantum wells.[5,6] Later simpler double CaF_2 barrier structures were developed where the single-quantum well was formed by a Si film.[7,8] The performance of these devices has been improved by special deposition techniques which reduce the dewetting of Si on CaF_2 films.[9,10] Other RTD structures use lattice matched CdF_2 as alternative material for the quantum well[11] while Si-based CdF_2/CaF_2 intersubband quantum cascade structures are realized to obtain electroluminescence at room temperature.[12] Both electroluminescence and photoluminescence (PL) have been observed for Si-based MnF_2/CaF_2 heterostructures, too.[13] Furthermore, CaF_2 tunneling barriers are also used in the field of spintronics for the spin injection from ferromagnetic Fe_3Si films into Si.[14,15] These CaF_2-based resonant tunneling devices perform excellently due to the high insulating quality of CaF_2 with negligible leakage currents.[16]

Furthermore CaF_2 films are used as buffer layers for many different Si-based structures, e.g., for II-VI films[17] as well as IV-VI films.[18,19] CaF_2 films are also passivating buffer layers for lattice matched CeO_2 films deposited on Si(111) to prevent the formation of amorphous silicate layers at the interface.[20,21] Finally, the very good passivating and insulating characteristics of CaF_2 films are also used for organic films of C_{60} molecules[22] or anthracene derivates.[23] In addition, CaF_2/Si(111) has been used to for the self-organization of atomic wires via selective adsorption of metal organic molecules at atomic steps of vicinal substrates.[24–26]

The key properties of CaF_2 films for all applications mentioned above are the large band gap and conduction-band offsets, respectively, as well as the high quality of ultrathin CaF_2 films deposited on Si(111). The latter point strongly depends on the lattice matching between CaF_2(111) and Si(111). Hence, it is necessary to clarify in detail the structure and morphology of CaF_2 films deposited on Si(111) as well as the structure of the interface between both materials and the relaxation of CaF_2 since these properties drastically influence the quality of CaF_2 tunneling barriers and buffer layers.

The structure of ultrathin CaF_2 films deposited on Si(111) and their interfaces has been investigated with various experimental techniques. However, there are only very few studies on the relaxation of these films. For instance, *in situ* studies by medium energy ion scattering (MEIS) performed after CaF_2 submonolayer deposition at *high* temperatures demonstrate that CaF_2 dissociates on the Si surface and forms a B-oriented CaF interface layer (i.e. 180° rotation of the CaF layer with respect to the [111] axis of Si(111); $CaF_2[11\bar{2}]\|Si[\bar{1}\bar{1}2]$) with Ca located on T_4 sites (cf. Fig. 1).[27] Furthermore, x-ray standing-wave (XSW) studies confirmed Ca adsorption on T_4 site for CaF submonolayers deposited at high temperature.[28] Klust *et al.* showed by means of XSW that Ca also adsorbs on T_4 sites for *low* deposition temperatures.[29] The formation of a CaF interface layer due to dissociation of CaF_2 at the Si(111) surface and subsequent desorption of SiF_x complexes has also been verified by x-ray photoelectron spectroscopy.[30,31] Furthermore, investigations by grazing incidence x-ray diffraction (GIXRD) verified both T_4 and H_3 adsorption sites for ultrathin CaF films if they are treated by rapid thermal annealing at *very high* temperatures after deposition.[32]

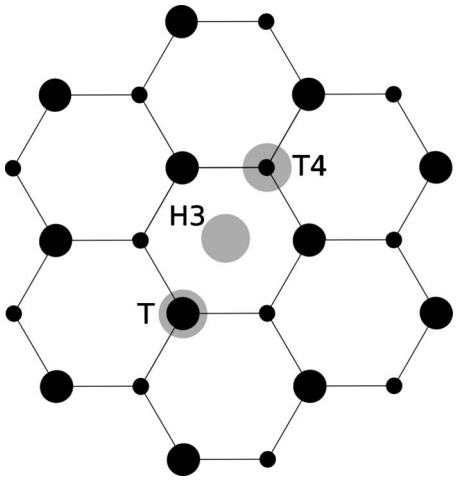

FIG. 1. Possible adsorption sites (gray circles) for the Ca ion of the CaF molecule on the Si(111) surface. Large black circles and small black circles represent the upper and lower Si atoms of the first Si bilayer, respectively.

While these studies on CaF submonolayers were performed under conditions of ultrahigh vacuum (UHV) the structure of ultrathin CaF_2 films has also intensively been studied *ex situ* by XRD with samples where the CaF_2 film was capped by a protecting amorphous Si film or where CaF_2 was even unprotected. Here, the existence of two different interfaces (short/long distances) are reported (cf. Refs. 3 and 4 and references therein). On one hand, the long-distance interface with Ca adsorbed on the *T* site has been observed after deposition of CaF_2 at low temperatures.[33–35] Therefore, this interface structure has initially been attributed to the nondissociated CaF_2 film with A orientation, i.e., no rotation of the CaF_2 structure with respect to the Si(111) substrate; $CaF_2[11\bar{2}]\|Si[11\bar{2}]$. On the other hand, both the long-distance interface as well as the short-distance interface are also determined from XRD studies on CaF_2 films deposited where the CaF interface is formed.[33–39] Partly, there have been proposed models with bilayers of CaF (Ref. 38) or even $CaSi_2$ (Ref. 40) at the interface. Later the formation of the long-distance interface has been attributed to a structural transition of the interface due to aging and incorporation of atoms via diffusion through defects of the CaF_2 films.[3,41] This transition needs days to months depending on the preparation of the CaF_2/Si(111) structure. Surprisingly, it has been

reported that the transition also takes place if the CaF_2 film is capped by several nanometers amorphous Si. Therefore well-defined CaF_2/Si(111) structures can only be investigated by *in situ* studies as presented here.

Sokolov *et al.* studied the *homogeneous* strain of CaF_2 films deposited under various conditions on Si(111) by means of PL.[33,42–44] The PL studies are performed at low temperatures and the results had been recalibrated to room temperature assuming the thermal-expansion coefficient for bulk CaF_2 and Si. Both tensile and compressive strain are reported for high- and low-temperature depositions, respectively, from these experiments as well as from XRD experiments determining the vertical lattice constants of CaF_2 films.[44] Furthermore, investigations by transmission electron microscopy (TEM) demonstrate that dislocations initially nucleate at atomic steps of the substrate[36–38] while thicker films and thicker CaF_2 islands (formed due to Stranski-Krastanov growth mode) show two-dimensional networks of dislocations.[36]

Here we present synchrotron based *in situ* GIXRD studies of ultrathin CaF_2 films deposited on Si(111) substrates via molecular-beam epitaxy (MBE) to avoid the difficulties of ambient conditions. The lateral lattice constants of the CaF_2 films is probed by in-plane diffraction while the vertical lattice constant as well as the interface distance between CaF_2 film and Si(111) are determined by analysis of crystal truncation rods (CTRs) which is based on kinematic diffraction theory.

II. EXPERIMENTAL

Si(111) substrates were cleaned by hydrofluoric acid to remove the native oxide and impurities. The clean surface was covered with a thin chemical oxide after exposure to hydrogen peroxide and then the samples were kept inside a methanol bath before transfer into the UHV. The substrates were annealed at 600 °C for 12 h and after that flash annealed at 900 °C in the UHV chamber to remove the thin chemical oxide and to assure a flat and clean surface. The 7×7 reconstruction of the surface was confirmed by low-energy electron diffraction (LEED). CaF_2 films were deposited on Si(111) by MBE evaporating highly purified CaF_2 from a graphite crucible which was heated by electron bombardment. The substrate was kept at 500 or 600 °C during deposition and, in addition, the deposition rate was kept below 0.2 triple layer (TL)/min to achieve smooth and flat films.[45] One TL of CaF_2 consists of one Ca monolayer located between two monolayers of Fluorine ions (7.84×10^{14}/cm^2 CaF_2 molecules).[46]

Thereafter the samples were transferred into an ion getter pumped baby chamber equipped with a Be dome to perform x-ray diffraction measurements at the beamline BW2 at HASYLAB/DESY with grazing incidence.[47] There, a six-circle diffractometer with vertical sample mount was used to conduct GIXRD experiments with x-ray photons of an energy of 10 keV ($\lambda=0.124$ nm) and the x-ray beam at an incidence angle of 0.3° well above the critical angle of total reflection of Si ($\alpha_c=0.15°$). The intensity of the diffracted x-ray beams was measured with a NaI scintillation detector.

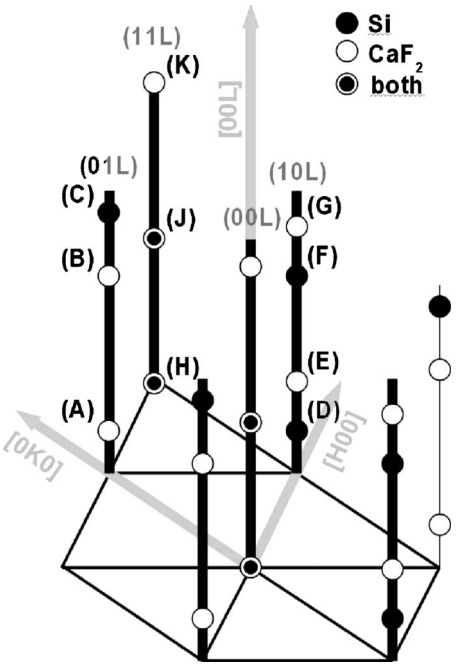

FIG. 2. Three-dimensional schematic view of the crystal truncation rods and the positions of the Bragg conditions of the B-type grown CaF_2 (open dots) with respect to the orientation of the Si substrate (black dots). See Table I for the notation in bulk and surface coordinate system.

III. RESULTS

GIXRD experiments have been performed to determine the morphology and structure of CaF_2 films and the structure of the interface between film and Si(111) substrate. The intensity distributions of the (01), (10), and (11) CTRs were studied to achieve information about film thickness, vertical lattice constants, and interface distances (cf. Fig. 2 and Refs. 48–50 for general information). In addition to this, the lateral intensity distributions (in-plane scans) close to Bragg conditions were analyzed to obtain information concerning lateral lattice mismatch, grain size, and lateral dispersion of different phases of the crystalline film.

A three-dimensional schematic view of the reciprocal space is presented in Fig. 2 in which the Bragg conditions of the substrate and B-oriented film are indexed assuming for reasons of simplicity that the film has the same lattice constants as the substrate has since CaF_2 is lattice matched to Si. The notations of the reciprocal-lattice points are given in Table I using the surface coordination system [with respect to the Si(111) substrate] and in the more common bulk notation (Miller indices) for the Si and the CaF_2 bulk, respectively. The matrix conversions from bulk to surface $[(H,K,L)_{surf}=M_{bulk\to surf}\cdot(H,K,L)_{bulk}]$ and vice versa $[(H,K,L)_{bulk}=M_{surf\to bulk}\cdot(H,K,L)_{surf}]$ between both notation systems can be done with the following matrices:

$$M_{surf\to bulk}=\begin{pmatrix} 2/3 & -2/3 & 1 \\ 2/3 & 4/3 & 1 \\ -4/3 & -2/3 & 1 \end{pmatrix}, \quad (1)$$

TABLE I. Bulk and surface notation for the Bragg conditions of Si substrate and B-oriented CaF_2 film (neglecting the very small lattice mismatch between both materials). The surface notation of the CaF_2 Bragg conditions are with respect to the coordinate system given by the Si substrate (cf. Fig. 2).

Index	Material	Bulk notation	Surface notation (Si)
(A)	CaF_2	$(1,\bar{1},1)$	$(0,1,\frac{1}{3})$
(B)	CaF_2	(2,0,2)	$(0,1,\frac{4}{3})$
(C)	Si	(1,3,1)	$(0,1,\frac{5}{3})$
(D)	Si	$(1,1,\bar{1})$	$(1,0,\frac{1}{3})$
(E)	CaF_2	(0,0,2)	$(1,0,\frac{2}{3})$
(F)	Si	(2,2,0)	$(1,0,\frac{4}{3})$
(G)	CaF_2	(1,1,3)	$(1,0,\frac{5}{3})$
(H)	Si, CaF_2	$(0,2,\bar{2})$, $(0,\bar{2},2)$	(1,1,0)
(J)	Si, CaF_2	$(1,3,\bar{1})$, $(1,\bar{1},3)$	(1,1,1)
(K)	CaF_2	(2,0,4)	(1,1,2)

$$M_{\text{bulk}\rightarrow\text{surf}} = \begin{pmatrix} 1/2 & 0 & -1/2 \\ -1/2 & 1/2 & 0 \\ 1/3 & 1/3 & 1/3 \end{pmatrix}. \quad (2)$$

In the following the surface notation will be used. The Bragg conditions pertaining to the Si substrate are located on the (10) rod at $L=1/3$ and $L=4/3$, on the (01) rod at $L=5/3$, and on the (11) rod at $L=0$ and $L=1$. The expected face-centered-cubic (fcc) Bragg conditions on the (01) rod at $L=2/3$ and on the (11) rod at $L=2$ vanish because of the symmetry of the diamond lattice.

One expects that the Bragg conditions of Si substrate and CaF_2 film are nearly at the same positions in reciprocal space due to the similar crystal structure (CaF_2: fluorite lattice and Si: diamond lattice) and approximately the same cubic lattice parameter (CaF_2: 546.2 pm and Si: 543.1 pm) (Ref. 2) with a lattice mismatch of only 0.58% at room temperature. It is well known, however, that CaF_2 molecules dissociate at the Si(111) surface and form CaF molecules and SiF_x complexes at the interface if CaF_2 is deposited at temperatures above 250 °C.[3,30,31,51,52] The dissociated CaF molecules adsorb with Ca on T_4 sites and the succeeding CaF_2 film grows with B orientation (cf. Ref. 3 and references therein). Thus the Bragg conditions of the CaF_2 film and Si substrate can be separated well for the (01) rod as well as for the (10) rod. As a result the Bragg conditions for the CaF_2 film are approximately located on the (10) rod at $L\simeq 2/3$ and $L\simeq 5/3$ and on the (01) rod at $L\simeq 1/3$ and $L\simeq 4/3$ due to the slightly larger vertical layer distance of the CaF_2(111) film compared to the Si(111) substrate. Firstly, this allows us to model the CTRs around the CaF_2 Bragg conditions more precisely and with negligible interference with the substrate signal. Secondly, the distinction of crystallite species (phases), which grow with different lateral lattice constants, can be done more definitely. For a direct comparison between the lateral lattice constants of substrate and film, however, one has to analyze the (11) rod by GIXRD, where the Bragg conditions of film and substrate do not separate so that interference effects between film and substrate are important.

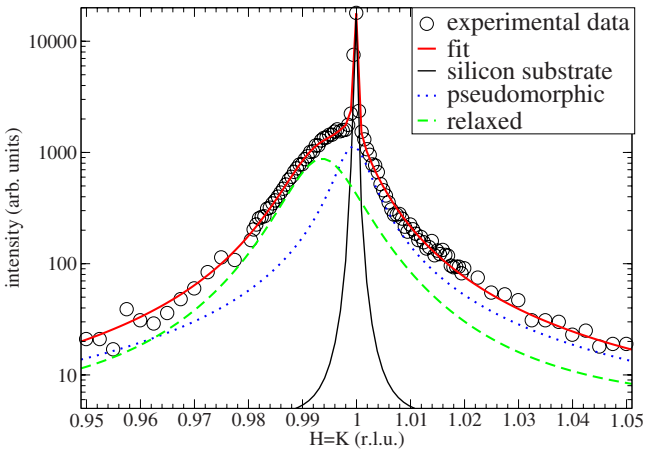

FIG. 3. (Color online) In-plane scan of the (11) rod at $L=0.08$. Circles denote data points while lines show the contributions of different CaF_2 phases and the Si substrate. The curve consists of three parts: the sharp Si substrate peak at $H=K=1.0$ surrounded by the intensity originated by the pseudomorphically grown CaF_2 and the peak of the relaxed grown CaF_2 located at $H=K=0.994$.

A. In-plane analysis

Figure 3 presents an in-plane scan ($[H,H,0]$ direction, cf. Fig. 2) of the (11) rod at $L=0.08$. The CaF_2 film of this sample was grown at a substrate temperature of 600 °C and had a thickness of 6.3 TL as verified by CTR measurements (see below).

One can clearly see the sharp and intense peak in the center due to the Si(111) substrate, which is surrounded by an asymmetric and broad peak due to the CaF_2 film. A closer inspection of the CaF_2 peak shows that the peak has two components at different lateral positions in reciprocal space. Therefore the CaF_2 film consists of two phases (crystallite species with different lateral lattice constants). The diffraction profile was fitted by three Lorentzian functions (one Lorentzian due to the Si substrate and two Lorentzians due to the two CaF_2 phases) to obtain the precise positions of the contributing peaks.

The first CaF_2 component, which is located on the lateral position of the substrate peak, mainly has its origin in the pseudomorphically grown CaF_2 phase which has assumed the lateral lattice constant of the Si(111) substrate. This assumption is verified by the CTR experiments presented below where fringes due to the finite film thickness are observed (cf. Figs. 5 and 7). However, it cannot entirely be excluded that a small amount of intensity is caused by diffuse scattering at the interface due to interface roughness. The second constituent induced by the CaF_2 film has its maximum at a position that is shifted by $\Delta H=\Delta K=-0.6\%$ to smaller K and H values. Since the same behavior is observed for $L=0.06-0.15$ we attribute the peak splitting to the formation of two phases of the CaF_2 film. The lateral lattice constant [distance between rows of the hexagonal (111) surface] of $a_{\text{rel}}=334.6(\pm 0.1)$ pm corresponding to the second

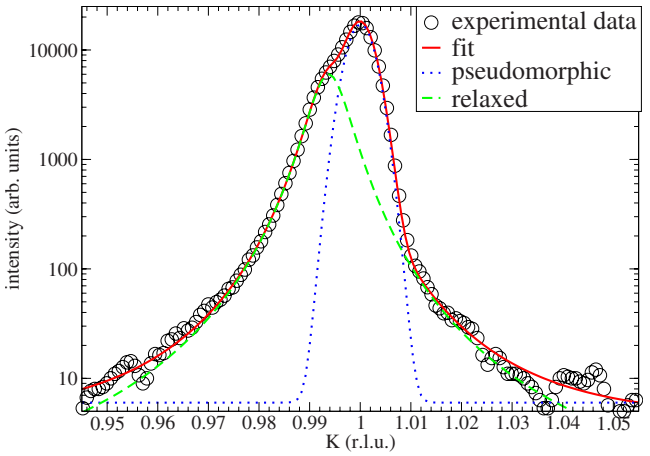

FIG. 4. (Color online) In-plane scan of the (01) rod at $L=0.38$. At $K=1.0$ the peak of the pseudomorphically grown CaF_2 is visible (dotted line). Shifted to lower K values the peak of the relaxed grown CaF_2 is located at $K=0.994$ (dashed line).

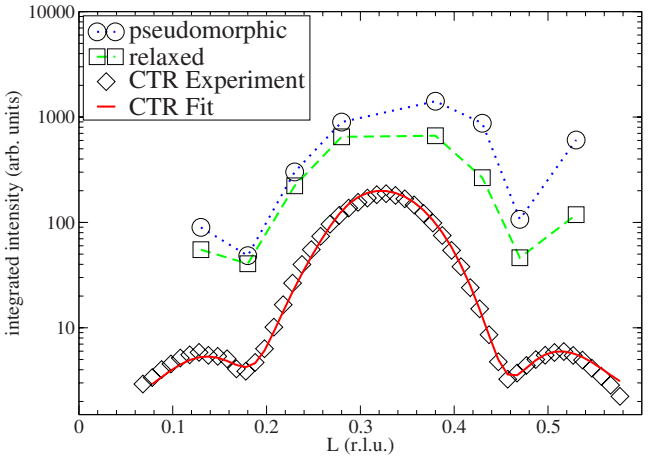

FIG. 5. (Color online) Integrated intensities of the diffraction peaks as determined from in-plane scans at different L values for the pseudomorphically (dashed line) and the relaxed (dotted line) grown CaF_2. The "all inclusive" CTR measured with open slits is given for comparison by diamonds while the best fit to the data points is shown as solid line.

phase matches the bulk lattice constant of $CaF_2(111)$. This is an evidence that a fraction of the CaF_2 film is laterally relaxed.

The ratio between the diffracted intensities of both crystallite species and therewith the ratio between the fractions of the two phases can be analyzed more easily at the CaF_2 Bragg condition on the (01) rod close to $L=1/3$. Here substrate effects can be excluded due to the B-type orientation of the CaF_2 film and the consequential separation of the Bragg conditions for the Si(111) substrate and the $CaF_2(111)$ film. Therefore, multiple in-plane scans have been performed on the (01) rod for the $[0,K,0]$ direction for $L=0.1-0.6$ (cf. schematic drawing presented in Fig. 2). All measurements show the same peak splitting of $\Delta K=-0.6\%$ due to the different CaF_2 phases (pseudomorphic and relaxed, respectively). For instance, Fig. 4 shows an in-plane scan of the (01) rod at $L=0.38$. One can see the same peak splitting caused by different lateral lattice constants as previously presented in Fig. 3 for the (11) rod except the missing sharp component due to the Si(111) substrate which vanishes here due to destructive interference between the layers of the Si substrate. The stronger peak is located at the expected position for the Si(111) substrate. Therefore this peak is caused by the pseudomorphic phase of the CaF_2 film. The weaker peak is shifted by 0.6% Brillouin zone to smaller K values, as expected for a completely relaxed grown CaF_2 film.

From the full width at half maximum (FWHM) one can estimate an average grain size of $\Gamma_{psm}=45(\pm 1)$ nm and $\Gamma_{rel}=37(\pm 1)$ nm for the pseudomorphically grown part and for the relaxed phase, respectively. The ratio between the relaxed and the pseudomorphically grown fraction of the CaF_2 film has been calculated from averaging the integrated intensities of the CaF_2 peaks for many different L values. In this case a quarter of the investigated CaF_2 film is relaxed while the residual pseudomorphic part of the film covers three quarters of the substrate.

B. Out-of-plane (CTR) analysis

Evaluating the intensities of the peaks due to both CaF_2 phases for different L values we can receive a CTR like intensity distribution for both components which is shown in Fig. 5 (upper part, circles and squares). The CTR curves run almost parallel pointing to the identical thickness of both fractions of the CaF_2 film. In addition, minima at $L=0.18$ and $L=0.46$ are observed. These minima point to fringes of the CTR curves which are better resolved in pure CTR measurement without lateral resolution (lower part of Fig. 5, diamonds). The fringes demonstrate that, firstly, the thickness of both phases is very homogeneous and that, secondly, the thickness of the film is approximately $2.1(\pm 0.2)$ nm. This result is supported from the FWHM of the CTRs of both phases which result in the same film thickness of $6(\pm 0.5)$ TL [equivalent to $1.9(\pm 0.2)$ nm] for both species. These results are in agreement with the result from the "standard" CTR analysis likewise given in Fig. 5. Thus, evidently, two different crystalline CaF_2 phases coexist *laterally*. The two CaF_2 species have the identical film thickness but different lateral lattice constants.

These measurements have also been performed for CaF_2 films of 3.3 TL thicknesses deposited at both temperatures 500 and 600 °C as well as a CaF_2 film of 7.0 TL thickness deposited at 600 °C. The results are presented in Table II. Obviously, the fraction of the relaxed CaF_2 film increases with increasing deposition temperature due to enhanced thermal relaxation processes. Furthermore, it also increases with increasing film thickness due to the larger stress for thicker films.

One has to record CTR intensities over a large range of L values to obtain more insight in the vertical structure of CaF_2 films. Therefore, we performed standard CTR experiments with open detector slits to measure the GIXRD intensity due to both phases (relaxed phase and pseudomorphic phase) which are at different positions in reciprocal space (cf. Fig. 5).

The intensity distribution along the (01), (10), and (11) rods were fitted by a simulation software based on the kinematic approximation of x-ray diffraction.[53] The fundamental

TABLE II. Structural parameters (cf. Fig. 6 for definition of the parameters) obtained from the CTR analysis of GIXRD experiments performed on CaF_2/Si(111). Defining the error of the parameters by an 10% increase in the goodness of fit R [cf. Eq. (3)] larger than the minimum value we obtain an error of 3 pm for c_{rel}, c_{psm}, and d_{int} while the error of $d_{CaF\text{-}CaF_2}$ is 6 pm.

Film thickness (TL)	Deposition temperature (°C)	Fraction of relaxed part (%)	c_{rel} (pm)	c_{psm} (pm)	d_{int} (pm)	$d_{CaF\text{-}CaF_2}$ (pm)
3.3	500	3	315.5	319.5	261.0	339.3
3.3	600	20	315.6	320.3	268.7	331.1
6.3	600	25	315.0	316.9	247.1	344.6
7.0	600	30	315.3	325.4	265.3	340.5

parameters, which can be obtained by this analysis, are the vertical lattice constant of the epitaxial film as well as interface distances. The GIXRD intensity, however, is also influenced by the roughness of interfaces and surfaces, respectively, and lattice vibrations (Debye-Waller factor).[49] For our analysis we assumed a Gaussian distribution of the roughness at the interface CaF_2-Si while we modeled the surface roughness of the CaF_2 film carefully adjusting the occupation of single CaF_2 surface layers. In agreement with the layer-by-layer growth of CaF_2 on Si(111) (Ref. 3) we obtain good results if we suppose that only the topmost CaF_2 layer is partly unoccupied (cf. the noninteger number of layers for the named film thickness). Furthermore the interface roughness is extremely small [rms roughness $w_{rms} \ll d_{Si}$, where d_{Si} denotes the Si(111) layer distance]. The very low values of surface and interface roughness can also be judged from the well developed CTR fringes which would be strongly damped if the roughness would be large.

The *goodness of fit* was quantified using the reliability factor R defined by

$$R = \sum_p [\log(I_p^{exp}) - \log(I_p^{calc})]^2, \quad (3)$$

where the summation p runs over all data points. I_p^{exp} and I_p^{calc} denote the experimental and calculated intensity, respectively, of this data point. In this reliability factor R the squared differences of the logarithmized intensities are summed to provide an uniform representation of all intensity regimes, from the substrate Bragg conditions to the much weaker fringes originated by the CaF_2 film of homogeneous thickness.

For the system investigated here we used two different models in which the two phases of the CaF_2 film are represented and which are shown in Fig. 6. Firstly, we studied a model where the pseudomorphic and the relaxed species are arranged vertically and their thicknesses are varied keeping the total thickness constant [Fig. 6 (I)]. The diffraction intensity is calculated from the *superposition of amplitudes* obtained from both components. And secondly, a model where the lateral coexistence is represented by two columns of nearly equal thickness [Fig. 6 (II)]. In this case the *amplitudes inside the columns* were added coherently and the resulting intensities of both columns were added incoherently (*superposition of intensities*) to obtain the final diffraction intensity. Both models include a CaF interface layer due to dissociation of CaF_2 molecules at the substrate temperatures used during deposition. For the two column model, however, it is assumed that only the pseudomorphic part of the CaF_2 film interferes with the Si(111) substrate since the Si substrate and the relaxed part of the CaF_2 film have different lateral lattice constants so that they do not fulfill the lateral Bragg conditions for identical lateral scattering vectors (separated CTRs of substrate and relaxed part of the film, cf. in-plane results). It has to be emphasized that finite-size effects due to the grain structure of the CaF_2 film leads to some residual diffraction effects of the relaxed CaF_2 phase with the Si CTR (cf. in-plane scan in Fig. 3). The amplitude of this signal, however, is very small since, firstly, only the wings of the diffraction from the relaxed CaF_2 contribute to the interference and, secondly, the fraction of the relaxed CaF_2 phase is small. Hence, the interface structure can only be deter-

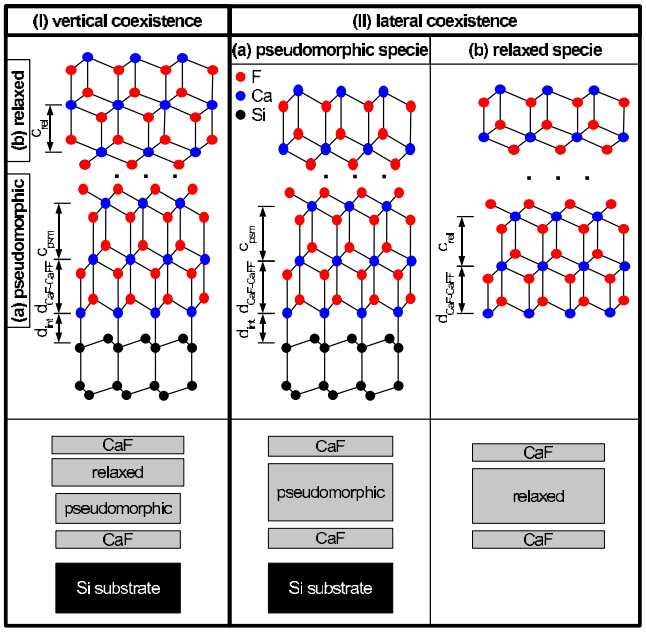

FIG. 6. (Color online) Schematic view of the two models used for the CTR simulation. (I) vertical coexistence and (II) lateral coexistence of the different CaF_2 species. For model (II) two columns are assumed: (a) the lateral lattice constant of the film is compressed due to the pseudomorphic growth so that the vertical lattice constant is expanded and (b) the lateral lattice parameter of the film does not fit the lateral Si lattice constant (relaxed phase). For the pseudomorphic column (a) the distance between the Si bilayer and the Ca atom of the CaF interface layer is given as d_{int} while the distances between the Ca atoms of two adjacent CaF_2 layers of the pseudomorphic part of the film is given by c_{psm}. This distance is denoted by c_{rel} for the relaxed column (b). In the latter case, the underlying Si substrate is not considered for the evaluation of the diffracted intensity since there is no well-defined phase relation between CaF_2 film and Si(111) substrate (random-phase approximation). In addition, the layer distance $d_{CaF\text{-}CaFF}$ between the CaF interface layer and the first CaF_2 layer is considered in the calculation.

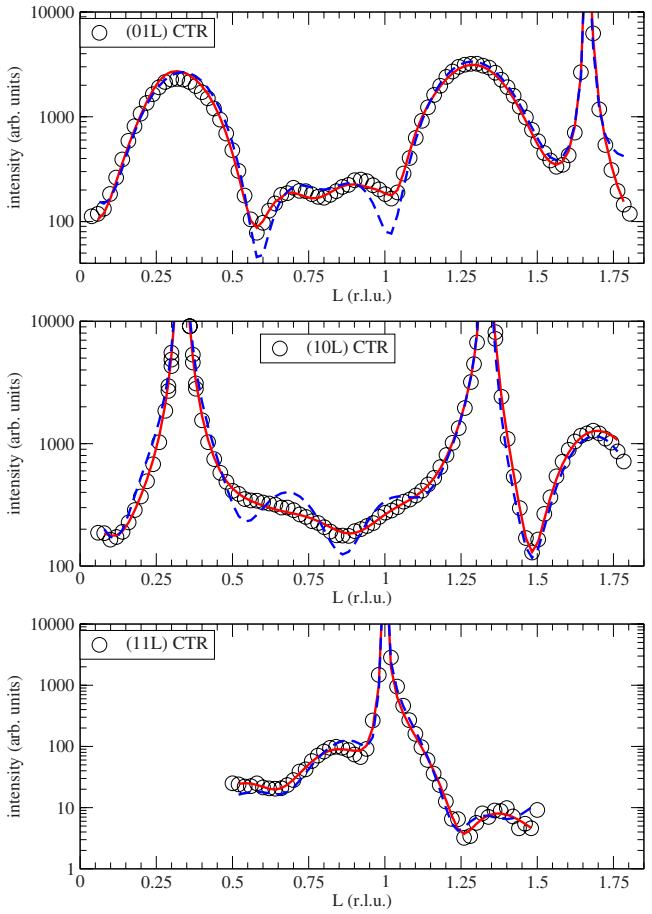

FIG. 7. (Color online) Measured data (open circles) and simulated intensity distribution (best fit) of the (01), (10), and (11) CTRs for the two different models: the vertical and the lateral coexistences of the pseudomorphically and the laterally grown CaF_2 species (dashed and solid lines, respectively).

mined for the pseudomorphic part of the CaF_2 film. Besides the interface structure of the relaxed part of the CaF_2 film is not well defined and may be distorted by interface dislocations (see below).

The results of the CTR simulation process are shown in Fig. 7 for a sample with a thickness of 3.3 TL. As one can clearly see, the adaptation of the lateral coexistence model (solid line) is much better than the best fit calculated with a vertical phase separation (dashed line). Especially in the ranges of $0.5 \leq L \leq 1.0$ of both the (10) and (01) rod the differences between both models are visible. The adaptation between measured data and simulation converged with a relative deviation of $R_{\mathrm{vert}}=19.5$ for the model of vertical coexistence and $R_{\mathrm{lat}}=8.9$ for the model of lateral coexistence. Therefore, this two column model has been applied to all samples studied here and the results are presented in Table II. All samples show similar structural parameters for the interface and the film (cf. Table II for details). We do not observe any specific trend of the structural data with respect to the deposition temperature nor to the film thickness. Therefore, we report here on the experimental results obtained from averaging the analysis of all these samples.

From the parameters of the model of lateral phase-separation one can achieve two vertical lattice constants for the CaF_2 film of $c_{\mathrm{psm}}=321(\pm 2)$ pm and $c_{\mathrm{rel}}=315(\pm 2)$ pm which can be assigned to the pseudomorphically grown and to the relaxed grown phase, respectively [cf. bulk value of $c_{\mathrm{bulk}}=315.3$ pm for $CaF_2(111)$]. The expanded vertical lattice constant of the pseudomorphic phase of the $CaF_2(111)$ film can be explained by the tetragonal elastic distortion of the film due to stress-strain behavior. Hashimoto *et al.* investigated the distortion of CaF_2 films with thickness ranging from several 10 nm to several 100 nm by Rutherford backscattering (RBS) and introduced the relationship

$$\frac{\Delta c}{c} = -A\frac{\Delta a}{a} \quad \text{with} \quad A = \frac{2\nu}{1-\nu} \tag{4}$$

for the tetragonal distortion of biaxial in-plane strained films. Here ν defines the Poisson ratio and the constant $A=0.958$ has been calculated from bulk elastic constants of CaF_2 ($\nu=0.324$).[54,55] Thus one expects a vertical expansion of 2 pm for the pseudomorphic CaF_2 phase at room temperature while we experimentally determine an expansion of $6(\pm 2)$ pm pointing to different elastic behavior of the CaF_2 film compared to its bulk elasticity. Consequently, we obtain $A=3.3(\pm 1.1)$ and $\nu=0.62(\pm 0.07)$ from the GIXRD experiments presented here.

Furthermore, we analyzed the interface structure between Si(111) substrate and the pseudomorphic phase of the $CaF_2(111)$ film. Firstly, we tested the CTR analysis for different adsorption sites of the Ca atom of the CaF interface film (not shown here). Our GIXRD study confirms that the interface Ca atoms are located on T_4 sites (cf. Fig. 1) as previously determined by different experimental techniques.[27,28,41] Secondly, the vertical distance between the Ca atoms of the CaF interface layer and the topmost Si atom of the Si bilayer located at the interface is $d_{\mathrm{int}}=255(\pm 7)$ pm while, thirdly, the upper Si half of the top Si bilayer shifts 5 pm towards the CaF_2 film with respect to the Si bulk values and, fourthly, the vertical distance between the Ca atoms of the CaF interface layer and the Ca atoms of the first CaF_2 layer is expanded [$d_{\mathrm{CaF\text{-}CaF_2}}=334(\pm 8)$ pm] with respect to the vertical lattice constant c_{psm} of the pseudomorphic CaF_2 phase.

The possible fraction of A-type grown parts of the CaF_2 film can excellently be determined from the (01) rod at $L \simeq 2/3$. No intensity due to the Si substrate can appear at this diffraction condition since the "expected" Si Bragg peak is forbidden due to the diamond structure of Si. Furthermore, A-oriented CaF_2 would show Bragg intensity here since it has fluorite structure. Our CTR analysis shows that the fraction of A-type grown CaF_2 is negligible in our experiments ($<1\%$).

Finally, the evaluation of the CTRs of the samples with a film thickness of 6.3 and 7.0 TL leads to structure models where the *surfaces* of the CaF_2 films consist of partial CaF layers, too, emphasizing the high sensitivity of GIXRD to interface and surface structures. These samples, however, were investigated by LEED at low-electron energies (<40 eV) after deposition of the CaF_2 films and prior to our GIXRD experiments. Thus the fluorine of the top CaF_2 surface layer have probably been removed via electron stimu-

lated desorption due to the Knotek Feibelmann mechanism[56] with threshold at 29 eV.[57–59]

IV. DISCUSSION

The GIXRD study on $CaF_2/Si(111)$ presented here offers information on the structure and relaxation of CaF_2 films grown epitaxially on Si(111) as well as the structure of the $CaF_2/Si(111)$ interface. The main conclusion of this report is the coexistence of different phases of the CaF_2 film with relaxed and pseudomorphic crystalline structure. On one hand, this result contradicts previous PL studies on $CaF_2/Si(111)$ in which strain effects of $CaF_2/Si(111)$ are studied supposing that the films are homogeneously strained.[33,42–44] On the other hand, this result is supported by TEM investigations (film thickness >3 nm) where *linear* areas of edge dislocations are observed and where it is assumed that edge dislocations are introduced at atomic substrate steps due to the incompatibility of Si(111) substrates and B-oriented $CaF_2(111)$ films.[36,38] Further TEM studies on CaF_2 films deposited at high temperatures ($T>700$ °C) demonstrate that CaF_2 films of 5 TL thickness are pseudomorphic while 15 TL films as well as Stranki-Krastanov islands show Moiré fringes due to *complete* relaxation of the film via (two-dimensional) dislocation networks.[36,37] Compared to these results, our GIXRD experiments demonstrate that CaF_2 films with thickness in the range of less than 3 nm are also *partly* relaxed. The films are inhomogeneous on the lateral scale (lateral phase separation) while the CaF_2 films are extremely homogeneous in vertical direction: both relaxed and pseudomorphic parts of the film have the same thickness.

Hashimoto *et al.*[54,55] studied the tetragonal distortion of CaF_2 films thicker than 30 nm, which were deposited at 700 °C, by RBS and observed a gradual decrease in the tetragonal distortion for films thinner than 250 nm *assuming* that the films are homogeneously strained. To explain the experimental results, they introduced a model with pseuodmorphic growth at deposition temperature so that the CaF_2 film, which is pinned at the interface, is compressively strained in lateral direction at room temperature due to the very different thermal-expansion coefficients α of both CaF_2 film and Si substrate ($\alpha_{CaF_2}=19\times10^{-6}/K$ and $\alpha_{Si}=2.5\times10^{-6}/K$). GIXRD experiments performed by Huang *et al.*[40] demonstrate that 5 nm CaF_2 films show lateral tensile strain if they are deposited at 700 °C. Therefore these experiments support the model of the lateral interface structure which is pinned due to the larger lattice mismatch at deposition temperature.

Our GIXRD studies, however, contradict this assumption since they show that the pseudomorphic part of films grown at 500 or 600 °C assumes the lateral lattice constant of Si at room temperature, too. Therefore there seems to exist a critical film thickness for the pinning of the lateral interface structure. Films with less than the critical thickness can partly rearrange their lateral interface structure and adopt the lateral structure of Si(111) substrates. Although the tetragonal distortion of $2.3(\pm0.6)\%$ in vertical direction we obtained for the pseudomorphic phase of the CaF_2 films studied here (film thickness 1.0–2.2 nm) is larger than the maximum tetragonal distortion of 1.6% reported by Hashimoto *et al.*[54,55] for films of 45 nm thickness this discrepancy can be explained by the reported increase in the tetragonal distortion for thinner film thicknesses.

The strain in ultrathin CaF_2 films on Si(111) has also been studied by PL. The CaF_2 films were doped by different rare-earth ions (e.g., Eu and Sm) for these studies. The PL experiments were performed at low temperatures and the results were recalibrated to room temperature assuming the thermal-expansion coefficients of the bulk material. It was also assumed that the tetragonal distortion of the CaF_2 film was homogeneous to determine the *lateral* strain of the CaF_2 films. Pseudomorphic growth was reported depositing 10 nm CaF_2 below 600 °C (Refs. 42 and 44) while the films already show tensile strain depositing 6 nm CaF_2 at 700 °C (Ref. 43) or 10 nm at 770 °C.[44] Pseudomorphic growth was also obtained if CaF_2 template films are deposited at low temperatures as 100 °C.[43] These results are compatible with the results obtained here since we observe almost no relaxed parts of the CaF_2 films deposited at 500 °C. Thus relaxation of the CaF_2 films is forced with increasing temperature.

The PL lines measured for films of small thickness were broad compared to CaF_2 bulk signals and the signal obtained from thick CaF_2 films deposited on Si(111) (film thickness several 100 nm). Therefore, it was concluded that the films have a high density of defects at the interface. This conclusion was amplified studying sequential doping of the CaF_2 films. Broad PL lines were obtained for doping the CaF_2 film close to the interface while doping close to the film surface led to sharp PL lines.[43] Our GIXRD results show that the defects at the interface are mainly due to the separation of ultrathin CaF_2 films into two phases of different lattice constants.

In addition, Alvarez *et al.*[44] combined synchrotron-based XRD studies with PL investigations to determine the lateral distortion of (homogeneous) CaF_2 films (film thickness 10 nm) which are deposited at different temperatures on Si(111). The CaF_2 films were capped by amorphous Si layers prior to demounting the samples from the MBE chamber. They conclude that films are compressively strained for deposition temperatures below 660 °C while they are completely relaxed for deposition at 660 °C. The lateral film distortion, however, was calculated from the *vertical* lattice distortion as determined from measuring the XRD intensity close to the (almost annihilated) $Si(222)_B$ (bulk) Bragg peak [equivalent to the $Si(002)_S$ (surface) Bragg peak]. If one recalculates the vertical lattice constant of the CaF_2 film from the reported degree of lateral strain one obtains that Alvarez *et al.* measure a vertical lattice constant of 317 pm for the 10 nm CaF_2 film deposited at 550 °C. Furthermore, Lucas *et al.*[41] also report a vertical lattice constant of 317.4 pm for an uncapped 10 nm CaF_2 film grown by a template procedure at 700 °C and studied by GIXRD. These results are close to the vertical lattice constant of 321 pm we obtained for the *pseudomorphic* part of thinner CaF_2 films deposited at 600 °C. We assume that the smaller vertical lattice constants reported for 10 nm CaF_2 films are due to the increasing relaxation of the film with increasing film thickness. A second contribution may be due to the assumption of the authors that the film is

homogeneous (one single phase) and exhibits only one (vertical) lattice constant. Therefore the influence of the smaller lattice constant of the nonconsidered relaxed part may decrease the *averaged* lattice constant to the smaller reported value.

It is quite surprising that we observe at least partial relaxation in the CaF_2 films studied here since the lattice mismatch of 0.58% at room temperature is very small so that one expects that the critical thickness as predicted by theory for the formation of dislocations and the relaxation of the film (cf. Ref. 60 and references therein) is rather larger than observed in our experiments. Here we follow the simplified theory of Nix who shows that the critical thickness can be estimated solving the equation

$$\frac{t_c}{b} = \frac{\ln(\beta t_c/b)}{8\pi(1+\nu)f}, \tag{5}$$

taking into account the elastic strain of stressed films and the formation energy of dislocations.[61] Here b denotes the length of the Burgers vector and the factor β equals roughly two. Assuming that relaxation occurs via Shockley partial dislocations $[b=|(11\bar{2})|a_0/6]$ one obtains the critical thickness $t_c=4.0(\pm 0.7)$ nm if the bulk Poisson ratio $\nu=0.324$ is valid. The critical thickness reduces to $t_c=3.0(\pm 0.4)$ nm for the Poisson ratio $\nu=0.62$ determined above for the CaF_2 film. Both values, however, are larger than the thickest films we studied here. Thus the critical thickness has to be reduced by additional effects. We like to mention that the theoretical critical thickness would even increase by a factor of $\sqrt{3}$ if one takes into account Burgers vector with $b=|(110)|a_0/2$ for complete dislocations.

Up to now, we neglected for the discussion of the relaxation process that all CaF_2 films studied here separate into two phases. The key point for the phase separation seems to be the B orientation of these films since the B orientation leads to nonmatching effects close to monoatomic Si(111) substrate steps.[45] Thus, on one hand, these steps act as growth barriers for the CaF_2 film. On the other hand, they are nucleation centers for the deposited CaF_2 film. Furthermore, it has been reported from AFM studies that CaF_2 forms rimlike structures close to buried substrate steps.[45] This result has been attributed to self-decoration effects due to relaxation of the CaF_2 film close to substrate steps. Thus substrate steps seem to enhance the nucleation probability of Shockley partial dislocations as reported for $CoSi_2$/Si(111) (Ref. 62) as well as CaF_2/Si(111) (Refs. 36 and 38) from TEM studies where dislocation bands close to substrate steps are reported. Therefore, we also attribute the phenomenon of lateral phase separation to the enhanced nucleation of Shockley partial dislocations close to substrate steps due to the B orientation of CaF_2 films. Perhaps, for these extremely thin films dislocations are not completely developed but can be considered as agglomeration of vacancies (preferentially at substrate steps) which may also decrease the nucleation barrier for dislocations. For increasing film thickness, the increased stress leads to an increased phase transformation to the relaxed film structure. Nevertheless, there seems to be a barrier that the entire film does not completely transform to the relaxed state. Starting from the substrate steps at the interface, the fraction of relaxed parts of the CaF_2 film grow over the adjacent *upper* terraces as concluded from growth experiments where an enhanced nucleation of CaF_2 close to substrate steps on the upper terrace is observed.[4,63]

Former XRD studies on B-oriented CaF_2 films on Si(111) often focused on the vertical lattice constant of the CaF_2 films and the interface distance between Si substrate and CaF interface film. Thus Lucas *et al.* report vertical lattice constants of approximately 317 pm for CaF_2 films with thickness from 3 to 13 nm and deposited in isothermal deposition as well as on high-temperature CaF_2 templates.[36–38,41] This vertical lattice constant is verified by Sokolov *et al.*, too.[33,35,39] These studies, however, were performed *ex situ* with CaF_2 films with or without capping layers under ambient conditions which may influence the lattice structure (especially if one takes into account structural changes at the interface, see below).[3,41,53]

Changes in the interface structure are heavily influenced due to exposure to ambient conditions. This effect is attributed to the diffusion of atoms from the gas phase to the interface via defects in the CaF_2 films.[3] There has been a comprehensive discussion concerning the formation of short and long interfaces.[3,33–39,41] This emphasizes the need of *in situ* studies as performed here. We obtain an interface distance of $d_{\mathrm{int}}=255(\pm 7)$ pm between the topmost Si atom and the Ca atom of the CaF interface layer.

On the one hand, the interface distance obtained here is clearly larger than the value of $d_{\mathrm{int}}=215(\pm 5)$ pm obtained for the CaF monolayer formed at high temperature as 770 °C and investigated *in situ* by MEIS.[27] It is also larger than the Ca-Si interface distance of $d_{\mathrm{int}}=229$ pm (taking into account the outward relaxation of the topmost Si interface layer) obtained by *in situ* XSW for CaF submonolayers deposited at 770 °C.[28] On the other hand, our result matches well the interface distance of 251 pm determined by XSW for deposition of 1.7 TL CaF_2 at 370 °C.[29] Therefore it seems that additional CaF_2 on top of the CaF interface layer increases the interface distance because of the attractive interaction between CaF interface layer and the CaF_2 layers of the film on top.

Furthermore, our *in situ* results for the interface distance are smaller than $d_{\mathrm{int}}=280(\pm 2)$ pm reported by Lucas *et al.*[37,41] for *ex situ* XRD studies on CaF_2 films of roughly 10 nm thickness and with the interface formed at high temperature. Similar values [248(±5) pm] to our results, however, are reported also for postdeposition annealed CaF_2 films which were deposited at 200 °C.[34] These XRD studies were performed a few days after preparation. Furthermore, Lucas *et al.*[41] report that the interface distance further increases to a value of 450 pm (long-distance interface) after exposure to ambient condition for 60 days. Therefore, it can be assumed that even the reported value of $d_{\mathrm{int}}=280(\pm 2)$ pm is larger than the interface distance of the virgin interface without any exposure to ambient conditions.

In literature, only little attention is payed to the binding between CaF interface layer and the first (lowest) CaF_2 layer of the CaF_2 film. On the one hand, Lucas *et al.* report a Ca-Ca distance of 318.4 pm for a 9 nm CaF_2 film grown by a template method (template deposited at high temperature,

further growth at low temperature). Klust *et al.* report from XSW experiments a similar distance of 320 pm for this structure. On the other hand, we obtain a slightly larger distance of 334 ± 8 pm. All values, however, agree with the expansion of this distance compared to both the layer distance of the CaF_2 bulk and the (contracted) interface distance.

V. SUMMARY

In summary, we studied *in situ* the structure and morphology of ultrathin CaF_2 films deposited on Si(111) substrates by means of GIXRD. The phase separation of domains with different lateral lattice constants (pseudomorphic and relaxed phases, respectively) has been concluded from the splitting in several peaks for in-plane diffraction scans. The vertical structure of the two phases has been determined from out-of-plane diffraction scans (CTR analysis) which confirm the formation of relaxed parts of the films although the films are smaller than the critical film thickness for relaxation as calculated from the theory of elastic strain and dislocation formation. This is attributed to the nucleation of Shockley partial dislocations at atomic substrate steps due to the B orientation of the CaF_2 film. The pseudomorphic part of the CaF_2 film is expanded in vertical direction due to the compressive lateral strain at the CaF-Si interface. The vertical expansion, however, is larger than expected from the Poisson ratio of the CaF_2 *bulk*. Therefore, we assume that the elastic properties of CaF_2 *films* differ from the properties of CaF_2 bulk. In addition, the interface structure of the pseudomorphic phase has been analyzed. In agreement with already reported results, it consists of a CaF monolayer with Ca on T_4 sites. On the one hand, the CaF-Si interface distance is smaller than the layer distances of both CaF_2 bulk and Si(111) bulk. On the other hand, the distance between the CaF interface layer and the first CaF_2 layer of the CaF_2 film is expanded.

*carsten.deiter@desy.de
†joachim.wollschlaeger@uos.de

[1] L. J. Schowalter and R. W. Fathauer, Crit. Rev. Solid State Mater. Sci. **15**, 367 (1989).
[2] W. Pies and A. Weiss, *Crystal and Solid State Physics*, Landolt-Börnstein, New Series, Group III Vol. 7 (Springer-Verlag, Berlin, 1973).
[3] M. A. Olmstead, *Thin Films: Heteroepitaxial Systems* (World Scientific, Singapore, 1999), p. 211.
[4] J. Wollschläger, *Recent Research Developments in Applied Physics* (Transworld Research Network, Trivandrum, India, 2002), Vol. 5-II, p. 621.
[5] T. Suemasu, M. Watanabe, M. Asada, and N. Suzuki, Electron. Lett. **28**, 1432 (1992).
[6] M. Watanabe, T. Suemasu, S. Muratake, and M. Asada, Appl. Phys. Lett. **62**, 300 (1993).
[7] M. Tsutsui, M. Watanabe, and M. Asada, Jpn. J. Appl. Phys., Part 2 **38**, L920 (1999).
[8] M. Watanabe, Y. Iketani, and M. Asada, Jpn. J. Appl. Phys., Part 2 **39**, L964 (2000).
[9] C. R. Wang, B. H. Müller, and K. R. Hofmann, Nanotechnology **14**, 1192 (2003).
[10] C. R. Wang, M. Bierkandt, S. Paprotta, T. Wietler, and K. R. Hofmann, Appl. Phys. Lett. **86**, 033111 (2005).
[11] M. Watanabe, T. Funayama, T. Teraji, and N. Sakami, Jpn. J. Appl. Phys., Part 2 **39**, L716 (2000).
[12] K. Jinen, T. Kikuchi, M. Watanabe, and M. Asada, Jpn. J. Appl. Phys. **45**, 3656 (2006).
[13] A. G. Banshchikov, S. V. Gastev, M. Ichida, A. Nakamura, H. Ofuchi, N. S. Sokolov, M. Tabuchi, Y. Takeda, N. L. Yakovlev, and M. V. Zamoryanskaya, J. Lumin. **87-89**, 519 (2000).
[14] T. Harianto, K. Kobayashi, T. Suemasu, and H. Akinga, Jpn. J. Appl. Phys., Part 2 **46**, L904 (2007).
[15] K. Kobayashi, T. Suemasu, N. Kuwano, D. Hara, and H. Akinga, Thin Solid Films **515**, 8254 (2007).
[16] N. S. Sokolov, A. K. Kaveev, A. V. Krupin, S. E. Tyaginov, M. I. Vexler, S. Ikeda, K. Tsutsui, and K. Saiki, Appl. Phys. Lett. **90**, 142909 (2007).
[17] T. Maruyama, N. Nakamura, and M. Watanabe, Jpn. J. Appl. Phys., Part 2 **41**, L876 (2002).
[18] S. P. Zimin, E. S. Gorlachev, I. I. Amirov, M. N. Gerke, H. Zogg, and D. S. Zimin, Semicond. Sci. Technol. **22**, 929 (2007).
[19] S. P. Zimin, E. A. Bogoyavlenskaya, E. S. Gorlachev, V. V. Naumov, D. S. Zimin, H. Zogg, and M. Arnold, Semicond. Sci. Technol. **22**, 1317 (2007).
[20] J. Zarraga-Colina, R. M. Nix, and H. Weiss, Surf. Sci. **563**, L251 (2004).
[21] J. Zarraga-Colina, R. M. Nix, and H. Weiss, J. Phys. Chem. B **109**, 10978 (2005).
[22] N. Iwata, A. Kinjo, H. Okuyama, and H. Yamamoto, Jpn. J. Appl. Phys. **44**, 617 (2005).
[23] H. Sasaki, Y. Wakayama, T. Chikyow, E. Barrena, H. Dosch, and K. Kobayashi, Appl. Phys. Lett. **88**, 081907 (2006).
[24] J. L. Lin, H. Rauscher, A. Kirakosian, F. J. Himpsel, and P. A. Dowben, J. Appl. Phys. **86**, 5492 (1999).
[25] J. L. Lin, D. Y. Petrovykh, A. Kirakosian, H. Rauscher, F. J. Himpsel, and P. A. Dowben, Appl. Phys. Lett. **78**, 829 (2001).
[26] K. Kametani, K. Sudoh, and H. Iwasaki, Jpn. J. Appl. Phys., Part 2 **41**, L1247 (2002).
[27] R. M. Tromp and M. C. Reuter, Phys. Rev. Lett. **61**, 1756 (1988).
[28] J. Zegenhagen and J. R. Patel, Phys. Rev. B **41**, 5315 (1990).
[29] A. Klust, M. Bierkandt, J. Wollschläger, B. H. Müller, T. Schmidt, and J. Falta, Phys. Rev. B **65**, 193404 (2002).
[30] D. Rieger, F. J. Himpsel, U. O. Karlsson, F. R. McFeely, J. F. Morar, and J. A. Yarmoff, Phys. Rev. B **34**, 7295 (1986).
[31] M. A. Olmstead, R. I. G. Uhrberg, R. D. Bringans, and R. Z. Bachrach, Phys. Rev. B **35**, 7526 (1987).
[32] K. G. Huang, J. Zegenhagen, J. M. Phillips, and J. R. Patel, Phys. Rev. Lett. **72**, 2430 (1994).
[33] N. S. Sokolov, T. Hirai, K. Kawasaki, S. Ohmi, K. Tsutsui, S. Furukawa, I. Takahashi, Y. Itoh, and J. Harada, Jpn. J. Appl. Phys. **33**, 2395 (1994).
[34] N. S. Sokolov, J. C. Alvarez, Y. V. Shusterman, N. L. Yakovlev,

R. M. Overney, Y. Itoh, I. Takahashi, and J. Harada, Appl. Surf. Sci. **104/105**, 402 (1996).
[35] J. Harada, I. Takahashi, Y. Itoh, N. S. Sokolov, N. L. Yakovlev, Y. V. Shusterman, and J. C. Alvarez, J. Cryst. Growth **163**, 31 (1996).
[36] C. A. Lucas and D. Loretto, Appl. Phys. Lett. **60**, 2071 (1992).
[37] G. C. L. Wong, D. Loretto, E. Rotenberg, M. A. Olmstead, and C. A. Lucas, Phys. Rev. B **48**, 5716 (1993).
[38] C. A. Lucas, G. C. L. Wong, and D. Loretto, Phys. Rev. Lett. **70**, 1826 (1993).
[39] Y. Itoh, I. Takahashi, A. Ichimiya, J. Harada, and N. S. Sokolov, J. Cryst. Growth **166**, 61 (1996).
[40] K. G. Huang, J. Zegenhagen, J. M. Phillips, and J. R. Patel, Physica B **221**, 192 (1996).
[41] C. A. Lucas, D. Loretto, and G. C. L. Wong, Phys. Rev. B **50**, 14340 (1994).
[42] N. S. Sokolov, N. L. Yakovlev, and J. Almeida, Solid State Commun. **76**, 883 (1990).
[43] N. S. Sokolov, S. V. Novikov, and N. L. Yakovlev, in *Insulating Films on Semiconductors 1991*, Proceedings from the 7th Biennial European Conference, edited by W. Eccleston (Hilger, Bristol, 1991), p. 203.
[44] J. C. Alvarez, K. Hirano, A. Y. Kazimirov, M. V. Kovalchuk, A. Y. Kreines, N. S. Sokolov, and N. L. Yakolev, Semicond. Sci. Technol. **7**, 1431 (1992).
[45] J. Wollschläger, Appl. Phys. A **75**, 155 (2002).
[46] T. Sumiya, Appl. Surf. Sci. **156**, 85 (2000).
[47] W. Drube, H. Schulte-Schrepping, H.-G. Schmidt, R. Treusch, and G. Materlik, Rev. Sci. Instrum. **66**, 1668 (1995).
[48] I. K. Robinson, Phys. Rev. B **33**, 3830 (1986).
[49] I. K. Robinson, R. T. Tung, and R. Feidenhans'l, Phys. Rev. B **38**, 3632 (1988).
[50] R. Feidenhans'l, Surf. Sci. Rep. **10**, 105 (1989).
[51] F. J. Himpsel, F. U. Hillebrecht, G. Hughes, J. L. Jordan, U. O. Karlsson, F. R. McFeely, J. F. Morar, and D. Rieger, Appl. Phys. Lett. **48**, 596 (1986).
[52] M. A. Olmstead and R. D. Bringans, J. Electron Spectrosc. Relat. Phenom. **51**, 599 (1990).
[53] C. Deiter, Ph.D. thesis, Universität Bremen, 2005.
[54] S. Hashimoto, J.-L. Peng, W. M. Gibson, L. J. Schowalter, and R. W. Fathauer, Appl. Phys. Lett. **47**, 1071 (1985).
[55] S. Hashimoto, L. J. Schowalter, R. W. Fathauer, and W. M. Gibson, *Layered Structures and Epitaxy*, MRS Symposia Proceedings No. 56 (Materials Research Society, Pittsburgh, 1986), p. 247.
[56] M. L. Knotek and P. J. Feibelman, Phys. Rev. Lett. **40**, 964 (1978).
[57] K. Miura, K. Sugiura, and H. Sugiura, Surf. Sci. **253**, L407 (1991).
[58] V. Chakarian, T. D. Durbin, P. R. Varekamp, and J. A. Yarmoff, Phys. Rev. B **48**, 18332 (1993).
[59] J. Wollschläger, T. Hildebrandt, R. Kayser, J. Viernow, A. Klust, J. Bätjer, A. Hille, T. Schmidt, and J. Falta, Appl. Surf. Sci. **162-163**, 309 (2000).
[60] I. Markov, *Crystal Growth for Beginners: Fundamentals of Nucleation, Crystal Growth, and Epitaxy* (World Scientific, Singapore, 2003).
[61] W. D. Nix, Metall. Trans. A **20**, 2217 (1989).
[62] R. T. Tung and F. Schrey, Appl. Phys. Lett. **54**, 852 (1989).
[63] J. Viernow, D. Y. Petrovykh, F. K. Men, A. Kirakosian, J. L. Lin, and F. J. Himpsel, Appl. Phys. Lett. **74**, 2125 (1999).